DISCRETE AND CONTINUOUS
DYNAMICAL SYSTEMS SERIES B
Volume **26**, Number **9**, September **2021**

doi:10.3934/dcdsb.2020311

pp. **4745–4765**

LOCAL STRUCTURE-PRESERVING ALGORITHMS FOR THE MOLECULAR BEAM EPITAXY MODEL WITH SLOPE SELECTION

Lin Lu

Jiangsu Key Laboratory for NSLSCS, School of Mathematical Sciences
Nanjing Normal University
Nanjing 210023, China

Qi Wang

Department of Mathematics
University of South Carolina
Columbia, SC 29208, USA

Yongzhong Song and Yushun Wang*

Jiangsu Key Laboratory for NSLSCS, School of Mathematical Sciences
Nanjing Normal University
Nanjing 210023, China

(Communicated by Jie Shen)

Abstract. Based on the local energy dissipation property of the molecular beam epitaxy (MBE) model with slope selection, we develop three, second order fully discrete, local energy dissipation rate preserving (LEDP) algorithms for the model using finite difference methods. For periodic boundary conditions, we show that these algorithms are global energy dissipation rate preserving (GEDP). For adiabatic, physical boundary conditions, we construct two GEDP algorithms from the three LEDP ones with consistently discretized physical boundary conditions. In addition, we show that all the algorithms preserve the total mass at the discrete level as well. Mesh refinement tests are conducted to confirm the convergence rates of the algorithms and two benchmark examples are presented to show the accuracy and performance of the methods.

1. **Introduction.** Molecular beam epitaxy (MBE) is a useful technique to grow crystal thin films [39, 19]. It has been widely used to produce high-electron mobility transistors and laser diodes. So far, this technique has been applied to a variety of industries, especially, to the semi-conductor and nano-technology industry. The molecular beam epitaxy model is one of the models used to model the process. It is a gradient flow model, derived from an energy variation procedure guided by the generalized Onsager principle or the second law of thermodynamics [15, 42, 43]. It admits the energy dissipation property both locally and globally. By local energy

2020 *Mathematics Subject Classification.* Primary: 65M06; Secondary: 80M20.

Key words and phrases. Molecular beam epitaxy model, local energy dissipation rate preserving, global energy dissipation rate preserving, mass conservation, structure-preserving, finite difference methods.

The first author is supported by NSFC grant 11771213, 61872422.

* Corresponding author: Yushun Wang.

dissipation, we refer to the fact that the energy density obeys a transport equation with a decay term and a flux term; while by the global energy dissipation, we refer to the total energy decaying in time subject to proper boundary conditions. The local energy dissipation is a structure issue for the energy density governing how energy decays locally and transfers through fluxes, while the global energy dissipation is a property of the system in general.

To respect the global energy dissipation property after the numerical discretization, one has developed numerical algorithms for the model, known as energy stable schemes. There have been quite a number of papers in the literature today discussing how to develop energy stable algorithms for phase field models including the MBE model. Here, we briefly recall some well-known strategies. One popular strategy is the convex splitting technique which has been studied and extended in [18, 30, 38, 40]. It requires one to decompose the free energy into a difference of two convex parts and to treat one implicitly while the other explicitly. However, we note that authors of [13] proposed an implicit nonlinear scheme and argued that the splitting error of convex splitting method might lead to misleading results. Another popular approach is the stablilizer technique, which has been used to derive energy stable schemes for phase field models as well as hydrodynamic models by Shen and Yang for a host of models [33, 41], in which a stabilizing term in the order of the scheme is added. In many cases, the stabilizer technique essentially deliver the effect as the convex splitting technique does by modifying the energy and/or the energy dissipation rate so that the energy decays in time. In 2011, Qiao et al. [28] proposed an adaptive time-stepping strategy for the MBE model to make the phase field simulation more accurate and efficient. Recently, a general approach to developing global energy dissipation rate preserving numerical algorithms via the energy quadratization approach has been developed. The resulting algorithms are known as EQ/IEQ/SAV schemes [44, 45, 32, 31, 12]. Another class method emerges to enforce global energy dissipation property using projection or supplementary variable methods [20, 21, 34, 11]. It is a common belief that if a numerical scheme for a PDE system warrants the global energy dissipation property, dynamics described by the PDE model would be better captured numerically. Hence, energy stable schemes can be viewed as a class of property/structure-preserving schemes.

For conservative systems like Hamiltonian systems, structure-preserving algorithms have achieved remarkable success in resolving long time dynamics and conservation. For instance, multi-symplectic formulation [1, 26, 29] provides an effective way for computing conservative PDEs based on their multi-symplectic geometry. To inherit the multi-symplectic structure, many multi-symplectic methods [2, 36, 17] are developed. In practices, it is easier to construct numerical algorithms that respect the energy conservation law than the symplectic or multi-symplectic structure [20]. Furihata [16] presented a discrete variational derivative method for a large class of PDEs that inherit energy conservation or dissipation properties. Celledoni et al. [10] used an averaged vector field method to construct a class of energy-preserving methods systemically based on the symplectic formulation of Hamiltonian PDEs. Based on the method of discrete line integrals, Brugnano et al. [3] proposed a Hamiltonian boundary value method, which can be recast as a multi-stage Runge-Kutta (RK) method. There are many other related works in this active research area which we cannot enumerate here, including the high-order energy-preserving and momentum-preserving algorithms etc. [25, 5, 14, 22, 4, 35, 23, 6].

In the past, most existing structure-preserving methods for dissipative PDEs focused on preserving the global energy dissipation property, represented by the energy stable schemes. These schemes preserve the dissipative property of the total energy in time. In addition to the total energy, the energy density, as another important physical variable, obeys a transport-decay equation deduced from the dissipative PDE system, whose spatial sum yields the global energy dissipation equation for the system. Preserving the structure of this energy density equation has not been put at the front burner when people address the energy stable issue for dissipative systems numerically. Notice that the ultimate goal of any numerical approximation is to design a numerical scheme for the PDE system so that the discrete equation system mimics the property and structure of the original (continuous) PDE system. In this study, we name the numerical scheme that preserves the structure of the energy density equation the local structure-preserving algorithm (SPA). In contrast, the one that preserves the global energy dissipation property of the PDE system is called the global structure-preserving algorithm. Under proper boundary conditions, one can show that a local SPA guarantees it's also a global SPA, but not the other way around. Hence, a local structure preserving approximation represents a refined and often better numerical approximation to a dissipative PDE system. In 2008, Wang et al. [37] proposed the concept of local structure preservation for conservative PDEs. To date, the methodology of local structure preservation has been applied to solve a wide class of PDE systems [7, 8, 17, 9, 27].

In this paper, we address the issue of preserving the structure of the energy density equation while developing numerical algorithms for a dissipative PDE system. We choose the MBE model with slope selection as an example. The methodology applies to general thermodynamically consistent models. We name the algorithm that preserves not only the structure of the energy density equation, but also the local energy decay/dissipation rate as the local energy dissipation rate preserving (LEDP) algorithm or scheme. We propose three new, second-order, LEDP algorithms/schemes for the dissipative MBE model. Since the global energy stability is a time-dependent issue, independent of any spatial discretization, the space discretization has been completely decoupled from the temporal discretization process before. However, the design of LEDP is dictated by how to discretize the equation in space properly. Therefore, we must discretize the space and time simultaneously in order to develop LEDP algorithms. One of our ideas is to introduce some intermediate variables to reformulate the original PDE system into one containing only the second order spatial gradients; then we apply a local energy dissipation preserving strategy to the reformulated system to arrive at local energy dissipation rate preserving algorithms [37]. Compared with the work in [27], the nonlinear term in the MBE model is more complex, which poses new challenges for us to construct the LEDP algorithms.

One of the technical challenges here is to develop a generalized, discrete Leibnitz rule in the first place. At the continuous level, one can derive the local energy dissipation law readily from the given dissipative PDE without reformulating the original system. However, it hardly works for the discrete case because we cannot derive the analogous local energy dissipation law with a discrete Leibnitz rule directly on the original PDE system. Hence, instead of rewriting the model into a first-order PDE system like in the previous works of Wang et al. [37, 7, 8, 17, 9, 27], we reformulate the model into an equivalent system with only second-order gradients by introducing intermediate variables. Based on the local energy dissipation

structure of the equivalent system, we apply the implicit midpoint method in both space and time, to arrive at our first scheme. Afterwards, we apply the implicit midpoint method and the Euler method to discretize the PDE model in both space and time to arrive at the other two schemes. We then prove rigorously that the resulting schemes preserve the local energy dissipation structure and property at the discrete level. In the case of periodic boundary conditions, we show readily that the proposed algorithms preserve mass conservation and global energy dissipation law (GEDL) simultaneously. At a physical boundary condition, like the adiabatic boundary condition however, one must carefully discretize the equation at different parts of the boundaries using different LEDP schemes; in the meantime, the free energy must be carefully defined and the boundary conditions discretized consistently with the PDE system in the domain in order to arrive at the global energy dissipation property. Extending the LEDP methodology to thermodynamically consistent PDEs, conservative and dissipative alike, to compact domains with physical boundary conditions represents a major advance in the development and implementation of the local structure-preserving algorithms. This paves the way for LEDP schemes to be used in simulations in bounded domains with physical boundary conditions.

The rest of the paper is organized as follows: in §2, we briefly discuss the properties of the MBE model with slope selection, with a special attention paid to the physical boundary conditions and their relation to the rate of energy dissipation. Three local energy dissipation rate preserving algorithms for the model are presented and discussed in §3; the construction of global energy dissipation rate preserving algorithms from the local energy dissipation rate preserving schemes will be discussed with respect to periodic and physical boundary conditions. In §4, we illustrate the accuracy and usefulness of the schemes using two benchmark numerical examples. A concluding remark is given in the final section.

2. MBE model with slope selection.

2.1. Formulation of the MBE model with slope selection.

We briefly review the derivation of the MBE model with slope selection using the generalized Onsager principle with a focus on its energy dissipation property and boundary conditions. The free energy of the MBE system in the model is given by

$$\mathcal{E}(\phi) = \int_\Omega \left(\frac{\epsilon^2}{2} |\Delta\phi|^2 + \frac{1}{4} \left(|\nabla\phi|^2 - 1 \right)^2 \right) \mathrm{d}\mathbf{x}, \tag{1}$$

where ϵ is a model parameter and ϕ is the dimensionless density.

The time rate of change of the free energy, i.e., the energy dissipation rate, is given by

$$\begin{aligned} \frac{\mathrm{d}\mathcal{E}}{dt} = & \int_\Omega \left\{ \left(\epsilon^2 \Delta^2 \phi - \nabla \cdot \left(\left(|\nabla\phi|^2 - 1 \right) \nabla\phi \right) \right) \cdot \phi_t \right\} \mathrm{d}\mathbf{x} \\ & + \int_{\partial\Omega} \left(\phi_t \left(|\nabla\phi|^2 - 1 \right) \nabla\phi \cdot \mathbf{n} + \epsilon^2 \Delta\phi \nabla\phi_t \cdot \mathbf{n} - \epsilon^2 \nabla\Delta\phi \cdot \phi_t \cdot \mathbf{n} \right) \mathrm{d}S. \end{aligned} \tag{2}$$

The energy dissipation rate is determined by two parts: the bulk contribution and the boundary contribution. Note that the chemical potential is defined by

$$\mu = \frac{\delta\mathcal{E}}{\delta\phi} = \epsilon^2 \Delta^2 \phi - \nabla \cdot \left(\left(|\nabla\phi|^2 - 1 \right) \nabla\phi \right). \tag{3}$$

If we choose the boundary conditions to satisfy

$$\phi_t \left(|\nabla\phi|^2 - 1\right) \nabla\phi \cdot \mathbf{n} + \epsilon^2 \Delta\phi \nabla\phi_t \cdot \mathbf{n} - \epsilon^2 \nabla\Delta\phi \cdot \phi_t \cdot \mathbf{n} = 0, \tag{4}$$

the energy dissipation rate reduces to

$$\frac{\mathrm{d}\mathcal{E}}{dt} = \int_\Omega \left\{ \left(\epsilon^2 \Delta^2 \phi - \nabla \cdot \left(\left(|\nabla\phi|^2 - 1 \right) \nabla\phi \right) \right) \cdot \phi_t \right\} \mathrm{d}\mathbf{x}, \tag{5}$$

which includes the bulk contribution exclusively. The sufficient conditions to ensure the above energy dissipation rate are

$$\mathbf{n} \cdot \nabla\phi = \mathbf{n} \cdot \nabla\Delta\phi = 0, \mathbf{x} \in \partial\Omega. \tag{6}$$

Applying the generalized Onsager principle, we obtain the MBE model with slope selection as follows

$$\begin{cases} \phi_t = -M\mu, \\ \mu = \epsilon^2 \Delta^2 \phi - \nabla \cdot \left((|\nabla\phi|^2 - 1) \nabla\phi \right), \\ \phi(\mathbf{x}, 0) = \phi_0(\mathbf{x}), \quad \mathbf{x} \in \Omega, \\ \mathbf{n} \cdot \nabla\phi = \mathbf{n} \cdot \nabla\Delta\phi = 0, \mathbf{x} \in \partial\Omega, \end{cases} \tag{7}$$

where $M \geq 0$ is the mobility coefficient.

2.2. **Property of the model.** Here, we show that Model (7) obeys a global energy dissipation law (GEDL) and a mass conservation law under proper boundary conditions and then derive the transport equation for the free energy density, which defines a local energy dissipation law (LEDL). Under the proper boundary conditions, we show that the LEDL implies a global energy dissipation law (GEDL).

Theorem 2.1. *Model (7) admits the following LEDL*

$$\partial_t E + \nabla \cdot (\epsilon^2 \nabla(\Delta\phi)\phi_t - \epsilon^2 \Delta\phi \nabla\phi_t - (|\nabla\phi|^2 - 1)\nabla\phi\phi_t) + M\mu^2 = 0, \tag{8}$$

where the energy density E is defined by

$$E = \frac{\epsilon^2}{2} |\Delta\phi|^2 + \frac{1}{4}(|\nabla\phi|^2 - 1)^2. \tag{9}$$

Proof. Multiplying the first line and second line of (7) by μ and ϕ_t, respectively, and adding the results, we have

$$\begin{aligned} -M\mu^2 = \nabla \cdot \left(\epsilon^2 \nabla(\Delta\phi)\phi_t - \epsilon^2 \Delta\phi \nabla\phi_t - \left(|\nabla\phi|^2 - 1 \right) \nabla\phi\phi_t \right) + \epsilon^2 \Delta\phi \cdot \Delta\phi_t \\ + \left(|\nabla\phi|^2 - 1 \right) \nabla\phi \cdot \nabla\phi_t. \end{aligned} \tag{10}$$

It follows from (9) that

$$\partial_t E = \epsilon^2 \Delta\phi \cdot \Delta\phi_t + \left(|\nabla\phi|^2 - 1 \right) \nabla\phi \cdot \nabla\phi_t. \tag{11}$$

Substituting (11) into (10), we arrive at the conclusion. □

We note that model (7) preserves mass and obeys the following global energy dissipation law (GEDL) [44],

$$\frac{\mathrm{d}}{\mathrm{d}t} \int_\Omega \phi(x,t) \mathrm{d}\mathbf{x} = 0, \quad \frac{\mathrm{d}}{\mathrm{d}t} \mathcal{E}(\phi) = -\frac{1}{M} \|\phi_t\|^2, \tag{12}$$

under the following boundary conditions

$$\mathbf{n} \cdot \nabla\phi|_{\partial\Omega} = 0, \quad \mathbf{n} \cdot \nabla(\Delta\phi)|_{\partial\Omega} = 0, \tag{13}$$

or the periodic boundary conditions. Here, the inner product and norm are defined respectively by

$$(\mathbf{F},\mathbf{G})=\sum_{m,n}\int_{\Omega}\mathbf{F}_{m,n}\mathbf{G}_{m,n}\mathrm{d}\mathbf{x},\quad \|\mathbf{F}\|=(\mathbf{F},\mathbf{F})^{\frac{1}{2}}. \tag{14}$$

where $\mathbf{F}$ and $\mathbf{G}$ are tensor functions in $L^2(\Omega)$.

Remark 1. Compared with the GEDL, defined by an integral, the LEDL is defined by an equation and is therefore independent of any boundary conditions. Under proper boundary conditions, e.g. periodic boundary conditions or boundary conditions given in (13), an LEDL (8) implies a GEDL.

2.3. **Model reformulation.** We reformulate model (7) into a system of equations with lower spatial derivatives by introducing the following intermediate variables

$$a=\epsilon^2\Delta\phi,\quad \mathbf{h}=\left(|\nabla\phi|^2-1\right)\nabla\phi, \tag{15}$$

$$\begin{cases}\phi_t=-M\mu,\\ \mu=-M\left(\Delta a-\nabla\cdot\mathbf{h}\right).\end{cases} \tag{16}$$

It is readily to show that system (15)-(16) respects the following LEDL

$$\partial_t E+\nabla\cdot\left(\nabla a\phi_t-a\nabla\phi_t-\mathbf{h}\phi_t\right)+M\mu^2=0, \tag{17}$$

where E is the energy density defined in (9).

Notice that this local energy dissipation law is equivalent to (8). However, the reformulation is essential for us to derive algorithms to preserve the LEDL at the discrete level next.

3. Local structure-preserving algorithms.

In this section, we design three local energy dissipation preserving algorithms for the model with slope selection, which are called **LEDP-I**, **LEDP-II** and **LEDP-III**, respectively. The design is guided crucially by the reformulated model.

Let N_x, N_y, N_t be three positive integers. We discretize the domain $\Omega_h = [x_L, x_R]\times[y_L, y_R]$ uniformly, with mesh sizes $h_x=(x_R-x_L)/N_x$, $h_y=(y_R-y_L)/N_y$. Then the grid points are given by the set

$$\Omega_h=\left\{(x_j,y_k)\middle| x_j=x_L+jh_x,\ y_k=y_L+kh_y,\ 0\le j\le N_x,\ 0\le k\le N_y\right\}. \tag{18}$$

The time interval $[0,T]$ is uniformly partitioned with step size $\tau=T/N_t$ to yield $t_n=n\tau, n=0,\cdots,N_t$. The approximate value of function $f(x,y,t)$ at node (x_j,y_k,t_n) is denoted by $f^n_{j,k}, j=0,\cdots,N_x, k=0,\cdots,N_y, n=0,\cdots,N_t$.

3.1. **Local energy dissipation preserving algorithm I (LEDP-I).** We discretize system (15)-(16) in both space and time using the implicit midpoint method to arrive at the following.

$$\begin{cases} \left\{ A_x^2 A_y^2 A_t a^n = \epsilon^2 \overline{\Delta}_h A_t \phi^n \right\}\Big|_{j,k}, & (19a) \\ \left\{ A_t A_x^2 A_y^2 \mathbf{h}^n = A_t \left(|\overline{\nabla}_h (A_x A_y \phi^n)|^2 - 1 \right) \overline{\nabla}_h (A_x A_y A_t \phi^n) \right\}\Big|_{j,k}, & (19b) \\ \left\{ \delta_t^+ A_x^2 A_y^2 \phi^n = -M (A_t A_x^2 A_y^2 \mu^n) \right\}\Big|_{j,k}, & (19c) \\ \left\{ A_t A_x^2 A_y^2 \mu^n = \overline{\Delta}_h A_t a^n - \overline{\nabla}_h \cdot (A_x A_y A_t \mathbf{h}^n) \right\}\Big|_{j,k}, & (19d) \end{cases}$$

where the operators are defined by

$$\begin{aligned} &A_t f_{j,k}^n = \frac{f_{j,k}^{n+1} + f_{j,k}^n}{2}, \quad A_x f_{j,k}^n = \frac{f_{j+1,k}^n + f_{j,k}^n}{2}, \quad A_y f_{j,k}^n = \frac{f_{j,k+1}^n + f_{j,k}^n}{2}, \\ &\delta_t^+ f_{j,k}^n = \frac{f_{j,k}^{n+1} - f_{j,k}^n}{\tau}, \quad \delta_x^+ f_{j,k}^n = \frac{f_{j+1,k}^n - f_{j,k}^n}{h_x}, \quad \delta_y^+ f_{j,k}^n = \frac{f_{j,k+1}^n - f_{j,k}^n}{h_y}, \\ &\overline{\nabla}_h = \begin{pmatrix} \delta_x^+ A_y \\ \delta_y^+ A_x \end{pmatrix}, \quad \overline{\Delta}_h = \overline{\nabla}_h \cdot \overline{\nabla}_h. \end{aligned} \tag{20}$$

We discretize energy density (9) at gird point (x_j, y_k) as follows

$$E^n = \frac{\epsilon^2}{2} |\overline{\Delta}_h \phi^n|^2 + \frac{1}{4} (|\overline{\nabla}_h (A_x A_y \phi^n)|^2 - 1)^2, \tag{21}$$

where we drop subscript (j, k) for simplicity.

Eliminating the intermediate variables, we obtain our first algorithm (**LEDP-I**) as follows:

Algorithm 1 (LEDP-I algorithm)**.**

$$\begin{aligned} &\delta_t^+ A_x^4 A_y^4 \phi^n \\ &= -M \left(\epsilon^2 \overline{\Delta}_h^2 A_t \phi^n - \overline{\nabla}_h A_x A_y \cdot \left(A_t \big(|\overline{\nabla}_h (A_x A_y \phi^n)|^2 - 1 \big) \overline{\nabla}_h (A_x A_y A_t \phi^n) \right) \right), \end{aligned} \tag{22}$$

where the spatial indices are (j, k), which are omitted for simplicity.

We next introduce some tools to prove the algorithm is local energy dissipation preserving.

Lemma 3.1. *For scalar functions f and g, we introduce the discrete Leibnitz rule*

$$\begin{aligned} \delta_x^+ (f \cdot g)_j &= f_j \cdot \delta_x^+ g_j + \delta_x^+ f_j \cdot g_{j+1}, \\ \delta_x^+ (f \cdot g)_j &= A_x f_j \cdot \delta_x^+ g_j + \delta_x^+ f_j \cdot A_x g_j, \\ \delta_x^- (f \cdot g)_j &= f_j \cdot \delta_x^- g_j + \delta_x^- f_j \cdot g_{j-1}. \end{aligned} \tag{23}$$

Analogously, we obtain the discrete Leibnitz rule in y as well as in time. We remark that the discrete Leibnitz rule plays an important role in constructing the algorithms that inherit the local energy dissipation law. Based on the discrete Leibnitz rule, we deduce the following properties. We omit the spatial indices in the following once again for simplicity.

Lemma 3.2. *For scalar functions f, g and vector functions $\mathbf{v}$, $\mathbf{u}$, with $\mathbf{v} = (v_1, v_2)^T$, we define $\nabla_h^\star \cdot$ as follows*

$$\nabla_h^\star \cdot (f^n \mathbf{v}^n) = \delta_x^+ \left(A_x A_y^2 f^n \cdot A_y v_1^n \right) + \delta_y^+ \left(A_x^2 A_y f^n \cdot A_x v_2^n \right), \tag{24}$$

the operator has the following property

$$\nabla_h^\star \cdot (f^n \mathbf{u}^n + g^n \mathbf{v}^n) = \nabla_h^\star \cdot (f^n \mathbf{u}^n) + \nabla_h^\star \cdot (g^n \mathbf{v}^n), \tag{25}$$

and it obeys the following discrete Leibnitz rule

$$\nabla_h^\star \cdot (f^n \mathbf{v}^n) = \overline{\nabla}_h (A_x A_y f^n) \cdot A_x A_y \mathbf{v}^n + A_x^2 A_y^2 f^n \cdot (\overline{\nabla}_h \cdot \mathbf{v}^n). \tag{26}$$

With the above lemmas, we now prove the following theorem.

Theorem 3.3. *Algorithm **LEDP-I** (22) satisfies the following discrete LEDL*

$$\begin{aligned} &\delta_t^+ E^n + \nabla_h^\star \cdot \left(\delta_t^+ \phi^n \cdot \overline{\nabla}_h (A_t a^n) - \delta_t^+ \phi^n \cdot A_t A_x A_y \mathbf{h}^n - A_t a^n \cdot \overline{\nabla}_h (\delta_t^+ \phi^n) \right) \\ &\quad + M |A_x^2 A_y^2 A_t \mu^n|^2 = 0. \end{aligned} \tag{27}$$

Proof. Multiplying (19c) and (19d) by $A_t A_x^2 A_y^2 \mu$ and $\delta_t^+ A_x^2 A_y^2 \phi^n$, respectively, and adding the results, we have

$$-M |A_x^2 A_y^2 A_t \mu^n|^2 = \overline{\Delta}_h A_t a^n \cdot \delta_t^+ A_x^2 A_y^2 \phi^n - \overline{\nabla}_h \cdot (A_t A_x A_y \mathbf{h}^n) \cdot \delta_t^+ A_x^2 A_y^2 \phi^n. \tag{28}$$

With the aid of lemma 3.2, we have

$$\begin{aligned} -M |A_x^2 A_y^2 A_t \mu^n|^2 = \nabla_h^\star \cdot &\left(\delta_t^+ \phi^n \cdot \overline{\nabla}_h (A_t a^n) - \delta_t^+ \phi^n \cdot A_t A_x A_y \mathbf{h}^n - A_t a^n \cdot \overline{\nabla}_h \delta_t^+ \phi^n \right) \\ &+ A_t A_x^2 A_y^2 a^n \cdot \overline{\Delta}_h \delta_t \phi^n + A_t A_x^2 A_y^2 \mathbf{h}^n \cdot \delta_t^+ \overline{\nabla}_h (A_x A_y \phi^n). \end{aligned}$$

It follows from Lemma 3.1 that

$$\delta_t^+ E^n = A_t A_x^2 A_y^2 a^n \cdot \delta_t^+ \overline{\Delta}_h \phi^n + A_t A_x^2 A_y^2 \mathbf{h}^n \cdot \delta_t^+ \overline{\nabla}_h (A_x A_y \phi^n).$$

Putting the above results together yields (27). □

For periodic boundary conditions, the LEDL implies the GEDL. For physical boundary conditions like (13), we must discretize the equation and the corresponding boundary conditions properly in order to ensure the LEDL implies the GEDL. This needs us to define the discrete free energy density that is consistent with the discretization methods. This is one important detail that one have to take care when dealing with LEDL. It's irrelevant for GEDL.

Next, we list some properties under periodic boundary conditions.

Lemma 3.4. *Let $V_h^p = \left\{ f_{j,k} | (x_j, y_k) \in \Omega_h,\ f_{j,k} = f_{j+N_x,k},\ f_{j,k} = f_{j,k+N_y} \right\}$ be the set of periodic grid functions on Ω_h. For $\forall\ f, \mathbf{v} \in V_h^p$, there exist the following identities*

$$\left(\overline{\nabla}_h \cdot \mathbf{v}^n, A_x A_y f^n \right)_h + \left(A_x A_y \mathbf{v}^n, \overline{\nabla}_h f^n \right)_h = 0,$$

$$\left(\overline{\nabla}_h (A_x A_y f^n), A_x A_y \mathbf{v}^n \right)_h + \left(A_x^2 A_y^2 f^n, \overline{\nabla}_h \cdot \mathbf{v}^n \right)_h = 0,$$

where the discrete inner product is defined by

$$(\mathbf{F}, \mathbf{G})_h = \sum_{m,n} \sum_{j=0}^{N_x - 1} \sum_{k=0}^{N_y - 1} (\mathbf{F}_{m,n})_{j,k} (\mathbf{G}_{m,n})_{j,k} h_x h_y. \tag{29}$$

The following properties follow from Lemma 3.4.

Corollary 3.1. *Under periodic boundary conditions, scheme (22) preserves total mass,*

$$\left(A_x^2A_y^2\phi^{n+1},1\right)_h=\left(A_x^2A_y^2\phi^{n},1\right)_h, \tag{30}$$

and the discrete energy dissipation law

$$\delta_t^+E_h^n+M\|A_tA_x^2A_y^2\mu^n\|_h^2=0, \tag{31}$$

where $E_h^n=\frac{\epsilon^2}{2}\|\overline{\Delta}_h\phi^n\|_h^2+\frac{1}{4}(\|\overline{\nabla}_h(A_xA_y\phi^n)\|_h^2-1)^2$ *and the discrete norm is defined as* $\|\mathbf{F}\|_h=(\mathbf{F},\mathbf{F})_h^{\frac{1}{2}}$.

3.2. **Local energy dissipation preserving algorithm II (LEDP-II) and III (LEDP-III).** We define the discrete energy density (9) as follows

$$E^n=\frac{\epsilon^2}{2}|\Delta_h\phi^n|^2+\frac{1}{4}\left(|\nabla_h^+\phi^n|^2-1\right)^2. \tag{32}$$

Applying the implicit midpoint method in time, the forward and backward Euler method in space to system (15)-(16), respectively, we obtain the following algorithm

$$\begin{cases}\left\{A_ta^n=\epsilon^2\Delta_hA_t\phi^n\right\}\Big|_{j,k}, & \text{(33a)}\\ \left\{A_t\mathbf{h}^n=A_t\left(|\nabla_h^+\phi^n|^2-1\right)A_t\nabla_h^+\phi^n\right\}\Big|_{j,k}, & \text{(33b)}\\ \left\{\delta_t^+\phi^n=-MA_t\mu^n\right\}\Big|_{j,k}, & \text{(33c)}\\ \left\{A_t\mu^n=A_t\Delta_ha^n-\nabla_h^-\cdot A_t\mathbf{h}^n\right\}\Big|_{j,k}, & \text{(33d)}\end{cases}$$

where the operators are defined as

$$\begin{aligned}&\delta_t^-f_{j,k}^n=\frac{f_{j,k}^n-f_{j,k}^{n-1}}{\tau},\quad \delta_x^-f_{j,k}^n=\frac{f_{j,k}^n-f_{j-1,k}^n}{h_x},\quad \delta_y^-f_{j,k}^n=\frac{f_{j,k}^n-f_{j,k-1}^n}{h_y},\\ &\nabla_h^+=\begin{pmatrix}\delta_x^+\\ \delta_y^+\end{pmatrix},\quad \nabla_h^-=\begin{pmatrix}\delta_x^-\\ \delta_y^-\end{pmatrix},\quad \Delta_h=\nabla_h^+\cdot\nabla_h^-.\end{aligned} \tag{34}$$

The system can be condensed into the following algorithm (**LEDP-II**).

Algorithm 2 (LEDP-II)**.**

$$\delta_t^+\phi^n=-M\left(\epsilon^2\Delta_h^2A_t\phi^n-\nabla_h^-\cdot\left(A_t(|\nabla_h^+\phi^n|^2-1)\nabla_h^+A_t\phi^n\right)\right). \tag{35}$$

The following lemma states a discrete Leibnitz rule for vector valued grid functions.

Lemma 3.5. *For scalar function* f *and vector function* $\mathbf{v}$*, we define vectors* $\overline{\mathbf{v}}_{j,k}^n=\left(v_{1_{j-1,k}}^n,v_{2_{j,k-1}}^n\right)^T$, $\widetilde{\mathbf{v}}^n=\left(v_{1_{j+1,k}}^n,v_{2_{j,k+1}}^n\right)^T$*, then we have the following discrete Leibnitz rules*

$$\begin{aligned}\nabla_h^+\cdot(f^n\mathbf{v}^n)&=(\nabla_h^+\cdot\mathbf{v}^n)\cdot f^n+\widetilde{\mathbf{v}}^n\cdot(\nabla_h^+f^n),\\ \nabla_h^+\cdot(f^n\overline{\mathbf{v}}^n)&=(\nabla_h^-\cdot\mathbf{v}^n)\cdot f^n+\mathbf{v}^n\cdot(\nabla_h^+f^n).\end{aligned} \tag{36}$$

Theorem 3.6. *Scheme* ***LEDP-II*** (35) *admits the discrete LEDL*

$$\begin{aligned}\delta_t^+ E^n + \nabla_h^+ \cdot \left(-\delta_t^+\phi^n \cdot A_t\overline{\mathbf{h}}^n + \delta_t^+\phi^n \cdot \nabla_h^- A_t a^n - \delta_t^+\nabla_h^-\phi^n \cdot A_t a^n\right) \\ + M\left|A_t\mu^n\right|^2 = 0,\end{aligned} \tag{37}$$

where $\overline{\mathbf{h}}_{j,k}^n = (f_{j-1,k}^n, g_{j,k-1}^n)^T$.

Proof. Analogous to the proof of Theorem 3.3, we multiply (33c) and (33d) by $A_t\mu^n$ and $\delta_t^+\phi^n$, respectively, and add the results to obtain

$$-M|A_t\mu^n|^2 = \Delta_h(A_t a^n)\cdot\delta_t^+\phi^n - \nabla_h^-\cdot(A_t\mathbf{h}^n)\cdot\delta_t^+\phi^n. \tag{38}$$

With the aid of lemma 3.5 and the definition of discrete energy density (32), we deduce (37). □

Similarly, we define the discrete energy density (9) by

$$E^n = \frac{\epsilon^2}{2}|\Delta_h\phi^n|^2 + \frac{1}{4}\left(|\nabla_h^-\phi^n|^2 - 1\right)^2. \tag{39}$$

We then apply the implicit midpoint method in time and the Euler method in space to system (15)-(16) to obtain another scheme

$$\begin{cases} \left\{A_t a^n = \epsilon^2\Delta_h A_t\phi^n\right\}\Big|_{j,k}, & \text{(40a)}\\ \left\{A_t\mathbf{k}^n = A_t\left(|\nabla_h^-\phi^n|^2 - 1\right)A_t\nabla_h^-\phi^n\right\}\Big|_{j,k}, & \text{(40b)}\\ \left\{\delta_t^+\phi^n = -MA_t\mu^n\right\}\Big|_{j,k}, & \text{(40c)}\\ \left\{A_t\mu^n = A_t\Delta_h a^n - \nabla_h^+\cdot A_t\mathbf{k}^n\right\}\Big|_{j,k}. & \text{(40d)}\end{cases}$$

The system can be simplified into the following algorithm (**LEDP-III**).

Algorithm 3 (LEDP-III)**.**

$$\delta_t^+\phi^n = -M\left(\epsilon^2\Delta_h^2 A_t\phi^n - \nabla_h^+\cdot\left(A_t(|\nabla_h^-\phi^n|^2 - 1)\nabla_h^- A_t\phi^n\right)\right). \tag{41}$$

Lemma 3.7. *For scalar function* f *and vector function* $\mathbf{v}$*, we define vectors* $\overline{\mathbf{v}}_{j,k}^n = \left(v_{1_{j-1,k}}^n, v_{2_{j,k-1}}^n\right)^T$, $\widetilde{\mathbf{v}}^n = \left(v_{1_{j+1,k}}^n, v_{2_{j,k+1}}^n\right)^T$*, then we have the following discrete Leibnitz rule*

$$\begin{aligned}\nabla_h^-\cdot(f^n\mathbf{v}^n) &= \nabla_h^-\cdot\mathbf{v}^n\cdot f^n + \nabla_h^- f\cdot\overline{\mathbf{v}}^n,\\ \nabla_h^-\cdot(f^n\widetilde{\mathbf{v}}^n) &= \nabla_h^-\cdot\widetilde{\mathbf{v}}^n\cdot f^n + \nabla_h^- f\cdot\mathbf{v}^n.\end{aligned} \tag{42}$$

Then, we have the following theorem for the third scheme.

Theorem 3.8. *Scheme* ***LEDP-III*** (41) *respects the discrete LEDL*

$$\begin{aligned}\delta_t^+ E^n + \nabla_h^-\cdot\left(-\delta_t^+\phi^n\cdot A_t\widetilde{\mathbf{k}}^n + \delta_t^+\phi^n\cdot\nabla_h^+ A_t a^n - \delta_t^+\nabla_h^+\phi^n\cdot A_t a^n\right) \\ + M\left|A_t\mu^n\right|^2 = 0,\end{aligned} \tag{43}$$

where $\widetilde{\mathbf{k}}_{j,k}^n = (f_{j+1,k}^n, g_{j,k+1}^n)^T$.

Proof. The proof is similar to Theorem 3.6 and is thus omitted. □

For periodic boundary conditions, the situation is simple.

Corollary 3.2. *Under periodic boundary conditions, schemes given in (35) and (41) preserve total mass*

$$\left(\phi^{n+1},1\right)_h=\left(\phi^n,1\right)_h, \tag{44}$$

and the discrete global energy dissipation law

$$\delta_t^+E_h^n+M\|A_t\mu^n\|_h^2=0, \tag{45}$$

*where E_h^n is defined by $E_h^n=\frac{\epsilon^2}{2}\|\Delta_h\phi^n\|_h^2+\frac{1}{4}\left(\|\nabla_h^+\phi^n\|_h^2-1\right)^2$ for **LEDP-II**, and $E_h^n=\frac{\epsilon^2}{2}\|\Delta_h\phi^n\|_h^2+\frac{1}{4}\left(\|\nabla_h^-\phi^n\|_h^2-1\right)^2$ for **LEDP-III**.*

3.3. **Schemes with physical boundary conditions.** When we use physical boundary conditions (13), the discretization of the equations as well as the corresponding boundary conditions must be done carefully in order for a LEDL to be a GEDL. In addition, the discrete free energy is defined differently from the one for the periodic boundary condition. At point (x_j,y_k,t_n), we denote the free energy density for scheme **LEDP-I**, **LEDP-II**, **LEDP-III** as $E^n_{1_{j,k}}$, $E^n_{2_{j,k}}$, and $E^n_{3_{j,k}}$, and the chemical potential μ in these schemes as $\mu^n_{1_{j,k}}$, $\mu^n_{2_{j,k}}$, $\mu^n_{3_{j,k}}$, respectively in this subsection.

Then, we delineate how we discretize the equations as well as the boundary conditions at the boundaries for the proposed schemes.

Proposition 3.1. *For **LEDP-I** alone, we cannot derive a GEDL from the LEDL under physical boundary conditions directly. We use **LEDP-I** at the upper and right boundary and **LEDP-II** at the bottom and left boundary, respectively. Namely, we discretize the equation near points $\{(x_j,y_k)\mid j=0 \text{ or } k=0\}$ with **LEDP-II**, and other places with **LEDP-I**. Consequently, the discrete total free energy is defined by the following*

$$E^{n'}_{1_h}=\sum_{j=1}^{N_x}\sum_{k=1}^{N_y}E^n_{1_{j,k}}+\left(\sum_{j=0}+\sum_{k=0}\right)E^n_{2_{j,k}}, \tag{46}$$

The boundary conditions are discretized as follows

$$\begin{aligned}&\overline{\nabla}_h a^n\cdot\mathbf{n}=0,\quad \overline{\nabla}_h\phi^n\cdot\mathbf{n}=0,\quad \forall\ (x_j,y_k)\in\{(x_j,y_k)\mid j=N_x \text{ or } k=N_y\},\\ &\overline{\nabla}_h\phi^n\cdot\mathbf{n}=0,\ \forall\ (x_j,y_k)\in\{(x_j,y_k)\mid j=N_x+2,N_x+3 \text{ or } k=N_y+2,N_y+3\},\end{aligned} \tag{47}$$

with $\overline{\nabla}_h a^n=\epsilon^2\left(\delta_x^{+3}A_yA_x^{-2},\delta_y^{+3}A_xA_y^{-2}\right)^T\phi^n$, and

$$\nabla_h^-\Delta_h\phi^n\cdot\mathbf{n}=0,\quad \nabla_h^-\phi^n\cdot\mathbf{n}=0,\quad \forall\ (x_j,y_k)\in\{(x_j,y_k)\mid j=0 \text{ or } k=0\}. \tag{48}$$

Then, we have the following GEDL consistent with our combined numerical scheme:

$$\delta_t^+E^{n'}_{1_h}+M\sum_{j=1}^{N_x}\sum_{k=1}^{N_y}|A_tA_x^2A_y^2\mu^n_{1_{j,k}}|^2+M\left(\sum_{j=0}+\sum_{k=0}\right)|A_t\mu^n_{2_{j,k}}|^2=0. \tag{49}$$

Proof. Summing up the free energy density at each point and inserting boundary conditions given in (47) and (48) into LEDL (27) and (37), respectively, we arrive at the GEDL. □

Proposition 3.2. *For **LEDP-II** and **LEDP-III**, we use them at different part of the domain in the following combinations:*

- *at* $\{(x_j, y_k) \mid j = N_x \text{ or } k = N_y\}$, *we use scheme* ***LEDP-III****, and other places we use* ***LEDP-II****;*
- *at* $\{(x_j, y_k) \mid j = 0 \text{ or } k = 0\}$ *we use scheme* ***LEDP-II****, and other places we use* ***LEDP-III****.*

The discrete free energy for each case is defined respectively by

$$\begin{aligned} E_{2_h}^{n'} &= \sum_{j=0}^{N_x-1}\sum_{k=0}^{N_y-1} E_{2_{j,k}}^{n} + \left(\sum_{j=N_x} + \sum_{k=N_y}\right) E_{3_{j,k}}^{n}, \\ E_{3_h}^{n'} &= \sum_{j=1}^{N_x}\sum_{k=1}^{N_y} E_{3_{j,k}}^{n} + \left(\sum_{j=0} + \sum_{k=0}\right) E_{2_{j,k}}^{n}. \end{aligned} \tag{50}$$

Discretizing the boundary conditions in both cases as follows:

$$\nabla_h^- \Delta_h \phi^n \cdot \mathbf{n} = 0, \quad \nabla_h^- \phi^n \cdot \mathbf{n} = 0, \quad \forall\ (x_j, y_k) \in \{(x_j, y_k) \mid j = 0 \text{ or } k = 0\}, \tag{51}$$

$$\nabla_h^+ \Delta_h \phi^n \cdot \mathbf{n} = 0, \quad \nabla_h^+ \phi^n \cdot \mathbf{n} = 0, \quad \forall\ (x_j, y_k) \in \{(x_j, y_k) \mid j = N_x \text{ or } k = N_y\}, \tag{52}$$

we deduce

$$\begin{aligned} &\delta_t^+ E_{2_h}^{n'} + M\sum_{j=0}^{N_x-1}\sum_{k=0}^{N_y-1} |A_t \mu_{2_{j,k}}^n|^2 + M\left(\sum_{j=N_x} + \sum_{k=N_y}\right) |A_t \mu_{3_{j,k}}^n|^2 = 0, \\ &\delta_t^+ E_{3_h}^{n'} + M\sum_{j=1}^{N_x}\sum_{k=1}^{N_y} |A_t \mu_{3_{j,k}}^n|^2 + M\left(\sum_{j=0} + \sum_{k=0}\right) |A_t \mu_{2_{j,k}}^n|^2 = 0, \end{aligned} \tag{53}$$

which imply the GEDL for both cases.

Proof. The proof is similar to the previous case and is thus omitted. □

The above discussion indicates that the discrete LEDL still implies the discrete GEDL even at physical boundary conditions. However, some adjustment in the method of discretization at certain parts of the boundaries, definition of the discrete energy etc. must be implemented carefully. In summary, we can deduce two discrete GEDL schemes using the combination of three discrete LEDL methods and modified definition of local energy density at proper parts of physical boundaries.

4. **Numerical results.** Note that scheme **LEDP-II** and scheme **LEDP-III** are similar. So we only conduct numerical experiments for **LEDP-I** and **LEDP-II** subject to periodic boundary conditions in this study. We conduct a mesh refinement test to verify the convergence rate firstly. We observe that proposed schemes (22) and (35) are all nonlinear, which can be solved by fixed-point iterative methods [17]. In every iteration step, with the help of periodic boundary conditions, we use fast Fourier transforms to speed up the computation. We define the error in the mass variable in **LEDP-I** and **LEDP-II**, respectively, as follows

$$\begin{aligned} RM_I^n &= |\left(A_x^2 A_y^2 \phi^n, 1\right)_h - \left(A_x^2 A_y^2 \phi^0, 1\right)_h|, \\ RM_{II}^n &= |\left(\phi^n, 1\right)_h - \left(\phi^0, 1\right)_h|. \end{aligned}$$

In order to numerically show the property of local energy dissipation, we define the maximal residue of the local energy dissipation rate for schemes **LEDP-I** and **LEDP-II**, respectively,

$$LE_I^{n+1/2} = \max_{j,k} \Big| \delta_t^+ E^n + \nabla_h^\star \cdot \left(\delta_t^+ \phi^n \cdot \overline{\nabla}_h \left(A_t a^n \right) - \delta_t^+ \phi^n \cdot A_t A_x A_y \mathbf{h}^n \right.$$
$$\left. - A_t a^n \cdot \overline{\nabla}_h \left(\delta_t^+ \phi^n \right) \right) + M |A_x^2 A_y^2 A_t \mu^n|^2 \Big|,$$
$$LE_{II}^{n+1/2} = \max_{j,k} \Big| \delta_t^+ E^n + \nabla_h^+ \cdot \left(-\delta_t^+ \phi^n \cdot A_t \overline{\mathbf{h}}^n + \delta_t^+ \phi^n \cdot \nabla_h^- A_t a^n - \delta_t^+ \nabla_h^- \phi^n \cdot A_t a^n \right)$$
$$+ M \left| A_t \mu^n \right|^2 \Big|.$$

Example 1 (Convergence rate test)**.** To test convergence rates of the two developed schemes, we make the following function solution of the system modified by an appropriate forcing term

$$\phi(x, y, t) = (\cos(x) + 1)(\cos(y) + 1)(\cos(t) + 1). \tag{54}$$

TABLE 1. Mesh refinement test for **LEDP-I** at $t = 1$.

N	τ	Error		Order		CPU time
		L^∞ error	L^2 error	L^∞ order	L^2 order	
11	0.1	0.1805	0.5671	–	–	6.24e-1
33	1/30	0.0170	0.0535	2.1495	2.1495	8.71e-1
99	1/90	0.0019	0.0058	2.0160	2.0160	4.82
297	1/270	2.0605e-4	6.4733e-4	2.0018	2.0018	5.75e+1
891	1/810	2.2890e-5	7.1910e-5	2.0002	2.0002	7.37e+2

TABLE 2. Mesh refinement test for **LEDP-II** at $t = 1$.

N	τ	Error		Order		CPU time
		L^∞ error	L^2 error	L^∞ order	L^2 order	
11	0.1	1.9180e-4	6.0195e-4	–	–	1.25e-1
33	1/30	2.1309e-5	6.6866e-5	2.0001	2.0002	2.47e-1
99	1/90	2.3678e-6	7.4296e-6	1.9999	2.0000	2.01
297	1/270	2.6376e-7	8.2575e-7	1.9977	1.9997	1.16e+1
891	1/810	2.9864e-8	9.1995e-8	1.9829	1.9976	8.79e+1

The parameter values used are $M = 1.0e-6$, $\epsilon^2 = 0.1$ and the computational domain is $[0, 2\pi] \times [0, 2\pi]$. We choose the number of spatial grids as $N_x = N_y = N$ and compare the numerical solution with the exact solution at $T = 1$. We compute L^∞ and L^2 errors of ϕ by varying the grid size in space and time simultaneously. From Table 1-2, we observe clearly that both schemes achieve second order accuracy in time and space. In the tables, we also recorded the CPU time used in the computations. The results show that the **LEDP-II** scheme performs at least twice as fast as the **LEDP-I** does.

Example 2. In this example, we use the codes developed from the two algorithms to simulate a benchmark MBE example in a periodic domain $[0, 2\pi]^2$ with 129^2 meshes and $\tau = 1.0e-3$. we set the initial condition as

$$\phi(x, y, 0) = 0.1\left(\sin 3x \sin 2y + \sin 5x \sin 5y\right), \tag{55}$$

and choose the values of parameters as $\epsilon^2 = 0.1$, $M = 1$.

In Figure 1, we show the contour lines of the numerical solution ϕ up to $t = 30$ by **LEDP-I** and **LEDP-II**, respectively. The simulation results agree well with the existing results in the literature [38, 44, 24]. Figure 2 shows the error in mass and energy from $t = 0$ to $t = 30$, where the insert shows the energy evolution for $t \in [0, 0.04]$. The numerical results indicate that the mass is numerically conserved by both schemes, while the energy decays with the same trajectory for both schemes. From Figure2(b), we observe that the energy for both schemes drop quickly at early time before it becomes steady. Based on this, we implemented an adaptive time-stepping method [28] using the following formula

$$\Delta t = max(\Delta t_{min}, \frac{\Delta t_{max}}{\sqrt{1 + \alpha[\|E'\|_\infty(t)]^2}}), \tag{56}$$

where E is the energy density.

In Figure 3, we illustrate the energy evolution for both schemes with constant time step $\Delta t = 1e-3$ and adaptive time-stepping methods. We show that both methods preserve the local energy dissipation rate and the adaptive time-stepping strategy works very well with the schemes. With the time adaptivity, the algorithms achieve similar accuracy with much reduced computational efforts as illustrated in Figure 1. The time step for using a constant $\Delta t = 1e-3$ is 30000 and it takes 732.05s and 144.97s for **LEDP-I** and **LEDP-II**, respectively. In Figure 3(a)(b), the time steps taken in the adaptive time-stepping method for **LEDP-I** are 85 and 73, and the CPU time is 14.55s and 14.39s for $\Delta t_{min} = 1e-3$ and $\Delta t_{min} = 1e-2$, respectively. In Figure 3(c)(d), the time steps in the adaptive time-stepping methods for **LEDP-II** are 85 and 139, and the CPU time is 13.93s and 15.89s for $\Delta t_{min} = 1e-3$ and $\Delta t_{min} = 1e-4$, respectively. This shows a significant improvement in computational efficiency using adaptive time stepping.

Example 3 (2D coarsening dynamics)**.** In this example, we perform numerical simulations of coarsening dynamics in 2D with the initial condition given as follows

$$\phi(x, y, 0) = 0.001 \cdot \text{rand}(x, y),$$

where $\text{rand}(x, y)$ generates random numbers in $[-1, 1]$. The simulations are carried out in the periodic domain $[0, L]^2$ with $L = 12.8$. We choose 513×513 meshes, parameter values $\epsilon = 0.03$ and $M = 1$ are used.

In Figure 4 and Figure 5, we show snapshots of numerical solutions of ϕ and its Laplacian $\Delta\phi$ at various time slots using **LEDP-I** and **LEDP-II**, respectively. We observe the growth of the epitaxial film where the pyramid/anti-pyramid shapes of hills and valleys. Figure 6 illustrates the error in mass, energy and maximal residue from $t = 0$ to $t = 80$. The numerical results show that both schemes conserve the total mass, while the energy decays with the same trajectory. Moreover, both schemes demonstrate excellent performance in preserving the local energy dissipation rate. Figure 7 illustrates the energy evolution of the two schemes via different time steps, from which we can see there is no signifigant difference while applying $dt = 1.0e-3, 1.0e-4$ *and* $1.0e-5$.

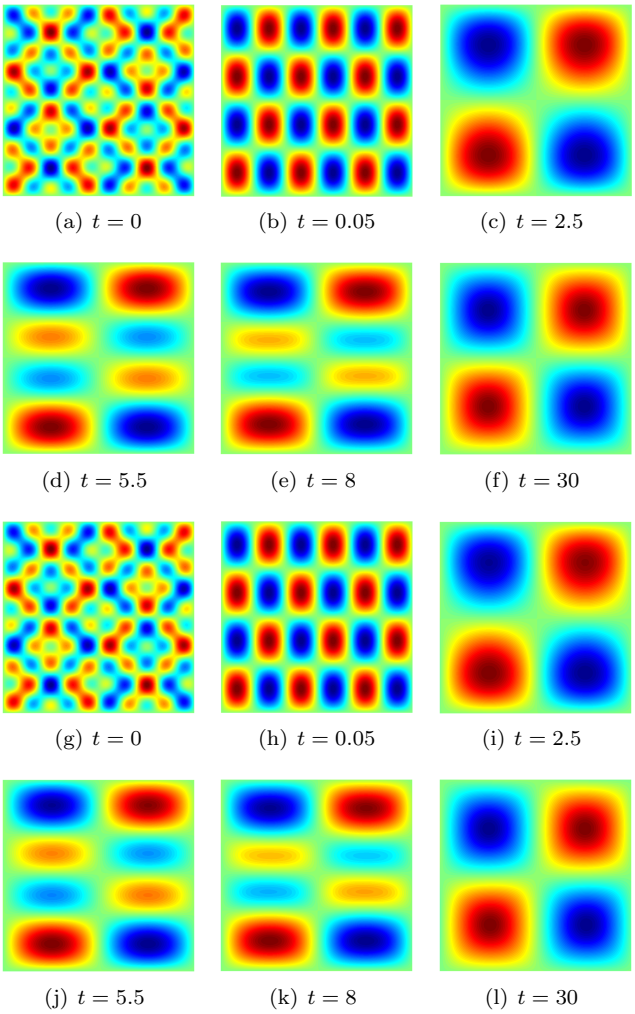

(a) $t = 0$ (b) $t = 0.05$ (c) $t = 2.5$

(d) $t = 5.5$ (e) $t = 8$ (f) $t = 30$

(g) $t = 0$ (h) $t = 0.05$ (i) $t = 2.5$

(j) $t = 5.5$ (k) $t = 8$ (l) $t = 30$

FIGURE 1. The isolines of numerical solutions of ϕ in Example 2 using **LEDP-I** and **LEDP-II**, respectively. (a-f) are obtained from **LEDP-I** while (g-l) from **LEDP-II**. Snapshots are taken at $t = 0, 0.05, 2.5, 5.5, 8, 30$, respectively. The time step is set as $\tau = 1.0e - 3$.

Define the roughness

$$W(t) = \sqrt{\frac{1}{|\Omega|}\int_{\Omega}\left(\phi(\mathbf{x},t) - \overline{\phi}\right)^2 \mathrm{d}\mathbf{x}}, \tag{57}$$

which is the standard deviation of the height profile, with $\overline{\phi} = \frac{1}{|\Omega|}\int_{\Omega}\phi(\mathbf{x},t)\mathrm{d}\mathbf{x}$. The discrete version of the roughness is

$$W(t_n) = \sqrt{\frac{h_x h_y}{(x_R - x_L)(y_R - y_L)}\sum_{j=0}^{N_x-1}\sum_{k=0}^{N_y-1}\left(\phi_{j,k}^n - \overline{\phi}^n\right)^2}. \tag{58}$$

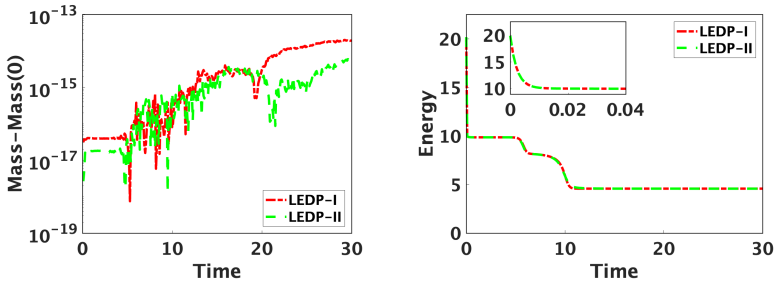

(a) Mass error (b) Energy

FIGURE 2. Time evolution of the error in mass and global energy with $N = 129$ and $\tau = 1.0e-3$ in Example 2 using **LEDP-I** and **LEDP-II**, respectively.

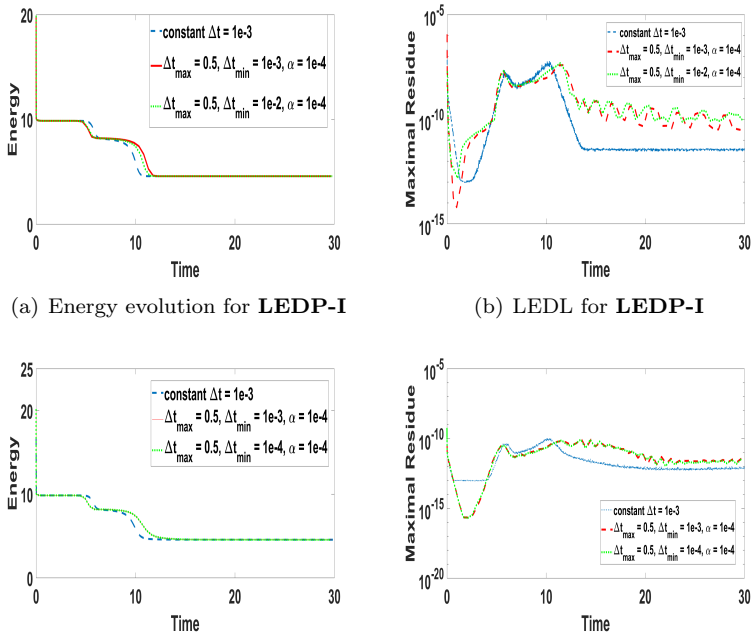

(a) Energy evolution for **LEDP-I** (b) LEDL for **LEDP-I**

(c) Energy evolution for **LEDP-II** (d) LEDL for **LEDP-II**

FIGURE 3. Time evolution of energy and maximal residue of the local energy dissipation law with $N = 129$, $\tau = 1.0e-3$ and τ based on adaptive time stepping algorithm in Example 2 using **LEDP-I**, **LEDP-II**, respectively.

As we know that coarsening dynamics of the MBE model follows a power law, where the energy decreases as $O(t^{-\frac{1}{3}})$, and the roughness increases as $O(t^{\frac{1}{3}})$ [38]. We show the energy decay and the roughness in Figure 8, which indicates a strong agreement with the expected power law. Therefore, these numerical results confirm that the

local energy dissipation preserving algorithms can be applied to predict accurate dynamics for this MBE model.

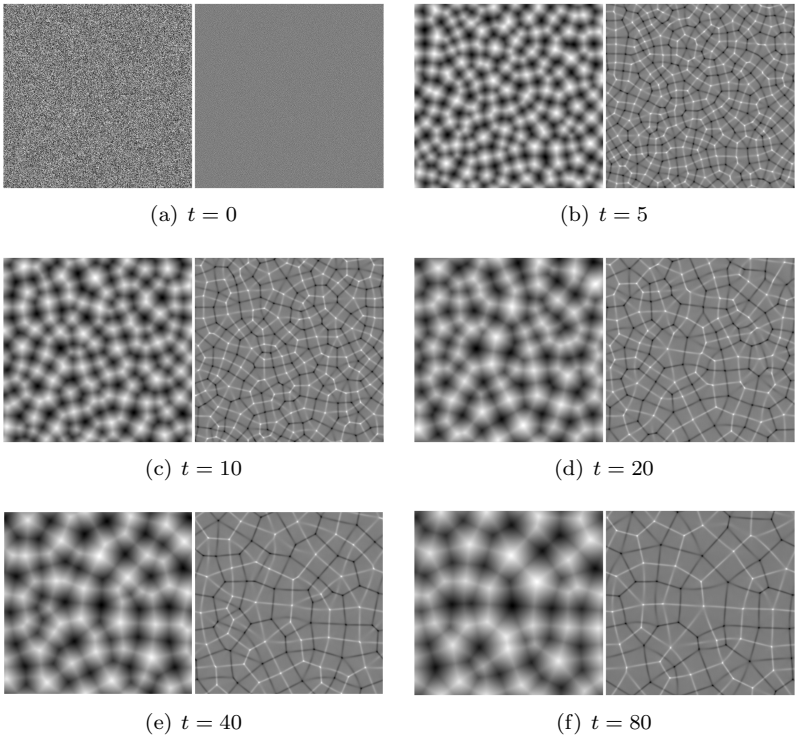

(a) $t = 0$ (b) $t = 5$

(c) $t = 10$ (d) $t = 20$

(e) $t = 40$ (f) $t = 80$

FIGURE 4. The isolines of numerical solutions of ϕ (left) and its Laplacian $\Delta\phi$ (right) in Example 3 using **LEDP-I**. Snapshots are taken at $t = 0, 5, 10, 20, 40, 80$. The time and space step are set as $\tau = 1.0e - 3$ and $N = 513$.

Remark 2. In the above examples, we implemented **LEDP-I** and **LEDP-II** using periodic boundary conditions, which are also GEDP schemes. When solving for solutions of the nonlinear algebraic systems resulted from the schemes, we used iterative methods and employed FFT to speed up the computation. For physical boundary conditions (13), the two GEDP schemes can also be implemented. However, FFT can no longer be used to solve the resulting linearized system of equations. Multigrid and other means would have to be considered in order to speed up the computation. How to implement the GEDP schemes with physical boundary conditions efficiently would be an issue we need to investigate throughout the future.

5. **Concluding remarks.** Based on the local energy dissipative structure of the MBE model with slope selection, we propose three second-order, LEDP algorithms for the model. To derive the algorithms, we firstly reformulate the original PDE into an equivalent form with only second-order gradients in space; then, we apply three second order discretization strategies in both space and time guided by the reformulated model to arrive at the LEDP algorithms. Under periodic boundary

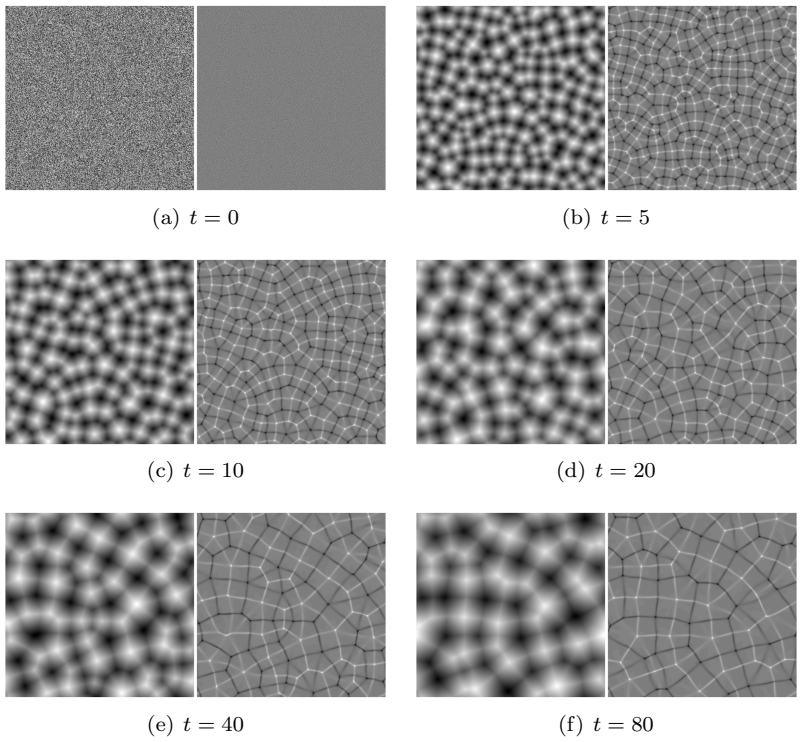

(a) $t = 0$ (b) $t = 5$

(c) $t = 10$ (d) $t = 20$

(e) $t = 40$ (f) $t = 80$

FIGURE 5. The isolines of numerical solutions of the ϕ (left) and its Laplacian $\Delta\phi$ (right) in Example 3 using **LEDP-II**. Snapshots are taken at $t = 0, 5, 10, 20, 40, 80$. The time and space step are set as $\tau = 1.0e-3$ and $N = 513$.

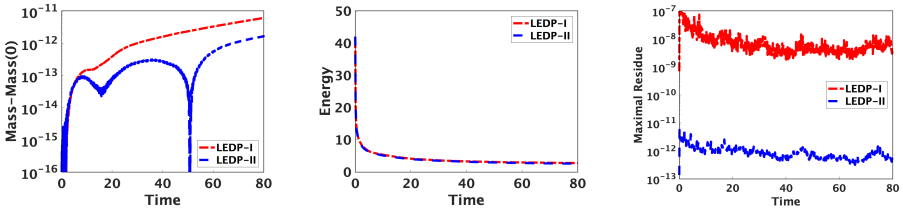

(a) (b) (c)

FIGURE 6. Time evolution of the error in mass, energy and maximal residue with $N = 513$ and $\tau = 1.0e-3$ in Example 3 using **LEDP-I** and **LEDP-II**, respectively.

conditions, the schemes are readily shown to preserve mass as well as the global energy dissipation property. For physical (adiabatic) boundary conditions, we apply combinations of the above LEDP schemes to construct two new LEDP schemes that are not only consistent with the boundary conditions but also globally energy preserving. Numerical experiments are given using the first two LEDP schemes to confirm that the schemes are second-order accurate in both space and time, and in

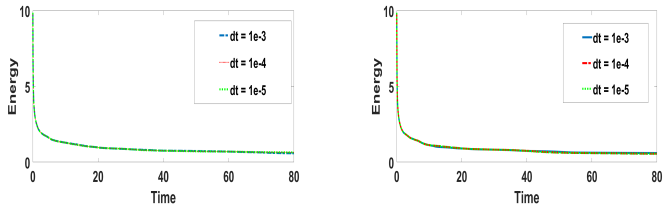

(a) Energy for **LEDP-I** (b) Energy for **LEDP-II**

FIGURE 7. The Energy for **LEDP-I** and **LEDP-II** via different time steps.

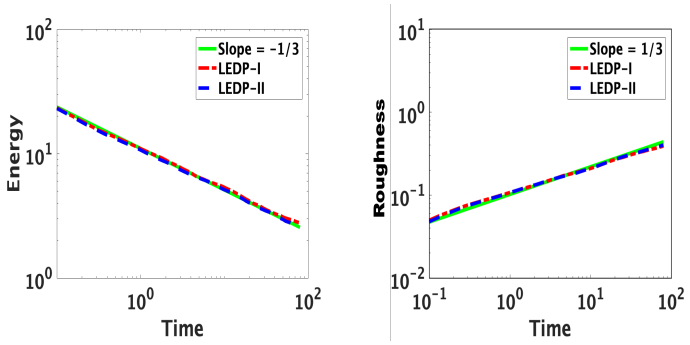

(a) Energy (b) Roughness

FIGURE 8. The numerical results show the proper power law behavior in the decaying energy as $O(t^{-\frac{1}{3}})$ and roughness as $O(t^{\frac{1}{3}})$.

the meanwhile preserve the local energy dissipation rate. Two benchmark examples are given to show the performance of the schemes with fixed time step sizes and adaptive time step sizes. The methodology developed in this study can be extended readily to general gradient flow models, which will be reported in a sequel.

Acknowledgments. This work is supported by the National Natural Science Foundation of China (Grant No.11771213, 61872422), the National Key Research and Development Project of China (Grant No.2018YFC1504205), the Major Projects of Natural Sciences of University in Jiangsu Province of China (Grant No.18KJA110003). Qi Wang's work is partially supported by National Science Foundationn (award DMS-1815921, DMS-1954532 and OIA-1655740), DOE DE-SC0020272 award and a GEAR award from SC EPSCoR/IDeA Program.

REFERENCES

[1] T. J. Bridges, Multi-symplectic structures and wave propagation, *Math. Proc. Cambridge Philos. Soc.*, **121** (1997), 147–190.

[2] T. J. Bridges and S. Reich, Numerical methods for Hamiltonian PDEs, *J. Phys. A*, **39** (2006), 5287–5320.

[3] L. Brugnano, F. Iavernaro and D. Trigiante, Hamiltonian boundary value methods (energy preserving discrete line integral methods), *JNAIAM. J. Numer. Anal. Ind. Appl. Math.*, **5** (2010), 17–37.
[4] L. Brugnano and Y. Sun, Multiple invariants conserving Runge-Kutta type methods for Hamiltonian problems, *Numer. Algorithms*, **65** (2014), 611–632.
[5] J. Cai, J. Hong, Y. Wang and Y. Gong, Two energy-conserved splitting methods for three-dimensional time-domain Maxwell's equations and the convergence analysis, *SIAM J. Numer. Anal.*, **53** (2015), 1918–1940.
[6] J. Cai and J. Shen, Two classes of linearly implicit local energy-preserving approach for general multi-symplectic Hamiltonian PDEs, *J. Comput. Phys.*, **401** (2020), 108975, 17 pp.
[7] J. Cai, Y. Wang and H. Liang, Local energy-preserving and momentum-preserving algorithms for coupled nonlinear Schrödinger system, *J. Comput. Phys.*, **239** (2013), 30–50.
[8] J. Cai and Y. Wang, Local structure-preserving algorithms for the "good" Boussinesq equation, *J. Comput. Phys.*, **239** (2013), 72–89.
[9] J. Cai, Y. Wang and C. Jiang, Local structure-preserving algorithms for general multi-symplectic Hamiltonian PDEs, *Comput. Phys. Comm.*, **235** (2019), 210–220.
[10] E. Celledoni, V. Grimm, R. I. McLachlan, D. I. McLaren, D. O'Neale, B. Owren and G. R. W. Quispel, Preserving energy resp. dissipation in numerical PDEs using the "average vector field" method, *J. Comput. Phys.*, **231** (2012), 6770–6789.
[11] Q. Cheng, C. Liu and J. Shen, A new lagrange multiplier approach for gradient flows, *Comput. Methods Appl. Mech. Engrg.*, **367** (2020), 113070, 20 pp.
[12] Q. Cheng, J. Shen and X. Yang, Highly efficient and accurate numerical schemes for the epitaxial thin film growth models by using the SAV approach, *J. Sci. Comput.*, **78** (2019), 1467–1487.
[13] A. Christlieb, J. Jones, K. Promislow, B. Wetton and M. Willoughby, High accuracy solutions to energy gradient flows from material science models, *J. Comput. Phys.*, **257** (2014), 193–215.
[14] N. Del Buono and C. Mastroserio, Explicit methods based on a class of four stage fourth order Runge–Kutta methods for preserving quadratic laws, *J. Comput. Appl. Math.*, **140** (2002), 231–243.
[15] M. Doi, Onsager's variational principle in soft matter, *J. Phys.: Condens. Matter*, **23** (2011), 284118.
[16] D. Furihata, Finite difference schemes for $\partial u/\partial t = (\partial/\partial x)^\alpha \delta G/\delta u$ that inherit energy conservation or dissipation property, *J. Comput. Phys.*, **156** (1999), 181–205.
[17] Y. Gong, J. Cai and Y. Wang, Some new structure-preserving algorithms for general multi-symplectic formulations of Hamiltonian PDEs, *J. Comput. Phys.*, **279** (2014), 80–102.
[18] Z. Guan, J. S. Lowengrub, C. Wang and S. M. Wise, Second order convex splitting schemes for periodic nonlocal Cahn-Hilliard and Allen-Cahn equations, *J. Comput. Phys.*, **277** (2014), 48–71.
[19] M. Guina and S. M. Wang, *Molecular Beam Epitaxy*, Elsevier, 2013.
[20] E. Hairer, C. Lubich and G. Wanner, *Geometric Numerical Integration: Structure-Preserving Algorithms for Ordinary Differential Equations*, Springer Series in Computational Mathematics, 31. Springer, Heidelberg, 2010.
[21] Q. Hong, J. Li and Q. Wang, Supplementary variable method for structure-preserving approximations to partial differential equations with deduced equations, *Appl. Math. Lett.*, **110** (2020), 106576, 9 pp.
[22] Q. Hong, Y. Wang and Y. Gong, Optimal error estimate of two linear and momentum-preserving Fourier pseudo-spectral schemes for the RLW equation, *Numer. Methods Partial Differential Equations*, **36** (2020), 394–417.
[23] L. Huang, Z. Tian and Y. Cai, Compact local structure-preserving algorithms for the nonlinear Schrödinger equation with wave operator, *Math. Probl. Eng.*, **2020** (2020), 4345278, 12 pp.
[24] B. Li and J. Liu, Thin film epitaxy with or without slope selection, *European J. Appl. Math.*, **14** (2003), 713–743.
[25] Y.-W. Li and X. Wu, Functionally fitted energy-preserving methods for solving oscillatory nonlinear Hamiltonian systems, *SIAM J. Numer. Anal.*, **54** (2016), 2036–2059.
[26] J. E. Marsden, G. W. Patrick and S. Shkoller, Multisymplectic geometry, variational integrators, and nonlinear PDEs, *Commun. Math. Phys.*, **199** (1998), 351–395.
[27] Z. Mu, Y. Gong, W. Cai and Y. Wang, Efficient local energy dissipation preserving algorithms for the Cahn-Hilliard equation, *J. Comput. Phys.*, **374** (2018), 654–667.

[28] Z. Qiao, Z. Zhang and T. Tang, An adaptive time-stepping strategy for the molecular beam epitaxy models, *SIAM J. Sci. Comput.*, **33** (2011), 1395–1414.
[29] S. Reich, Multi-symplectic Runge-Kutta collocation methods for Hamiltonian wave equations, *J. Comput. Phys.*, **157** (2000), 473–499.
[30] J. Shen, C. Wang, X. Wang and S. M. Wise, Second-order convex splitting schemes for gradient flows with Enrich-Schwoebel type energy: Application to thin film epitaxy, *SIAM J. Numer. Anal.*, **50** (2012), 105–125.
[31] J. Shen and J. Xu, Convergence and error analysis for the scalar auxiliary variable (SAV) schemes to gradient flows, *SIAM J. Numer. Anal.*, **56** (2018), 2895–2912.
[32] J. Shen, J. Xu and J. Yang, The scalar auxiliary variable (SAV) approach for gradient flows, *J. Comput. Phys.*, **353** (2018), 407–416.
[33] J. Shen and X. Yang, B. Wetton and M. Willoughby, Numerical approximations of Allen-Cahn and Cahn-Hilliard equations, *Disc. Conti. Dyn. Syst. Ser. A*, **28** (2010), 1669–1691.
[34] S. Sun, J. Li, J. Zhao and Q. Wang, Structure-preserving numerical approximations to a non-isothermal hydrodynamic model of binary fluid flows, *J. Sci. Comput.*, **83** (2020), 50, 43 pp.
[35] W. Tang and Y. Sun, Time finite element methods: A unified framework for numerical discretizations of ODEs, *Appl. Math. Comput.*, **219** (2012), 2158–2179.
[36] Y. Wang and J. Hong, Multi-symplectic algorithms for Hamiltonian partial differential equations, *Commun. Appl. Math. Comput*, **27** (2013), 163–230.
[37] Y. Wang, B. Wang and M. Qin, Local structure-preserving algorithms for partial differential equations, *Sci. China Ser. A*, **51** (2008), 2115–2136.
[38] C. Wang, X. Wang and S. M. Wise, Unconditionally stable schemes for equations of thin film epitaxy, *Discrete Contin. Dyn. Syst.*, **28** (2010), 405–423.
[39] A. Willoughby and P. Capper, *Molecular Beam Epitaxy: Materials and Applications for Electronics and Optoelectronics*, Springer, 2019.
[40] S. M. Wise, C. Wang and J. S. Lowengrub, An energy-stable and convergent finite-difference scheme for the phase field crystal equation, *SIAM J. Numer. Anal.*, **47** (2009), 2269–2288.
[41] X. Yang, Error analysis of stabilized semi-implicit method of Allen-Cahn equation, *Disc. Contin. Dyn. Syst. Ser. B*, **11** (2009), 1057–1070.
[42] X.-G. Yang, M. G. Forest and Q. Wang, Near equilibrium dynamics and one-dimensional spatial-temporal structures of polar active liquid crystals, *Chin. Phys. B*, **23** (2014), 118701.
[43] X. Yang, J. Li, M. G. Forest and Q. Wang, Hydrodynamic theories for flows of active liquid crystals and the generalized Onsager principle, *Entropy*, **18** (2016), 202, 28 pp.
[44] X. Yang, J. Zhao and Q. Wang, Numerical approximations for the molecular beam epitaxial growth model based on the invariant energy quadratization method, *J. Comput. Phys.*, **333** (2017), 104–127.
[45] J. Zhao, Q. Wang and X. Yang, Numerical approximations for a phase field dendritic crystal growth model based on invariant energy quadratization approach, *Internat. J. Numer. Methods Engrg.*, **110** (2017), 279–300.

Received March 2020; revised August 2020.

E-mail address: LL27@mailbox.sc.edu
E-mail address: qwang@csrc.ac.cn
E-mail address: yzsong@njnu.edu.cn
E-mail address: wangyushun@njnu.edu.cn